water

MDPI

Article

Efficient Removal of Phosphate, Nitrate, and Ammonia from Wastewater Using Unmodified Woodchip Biochar

Amani Haddouk [1,2], Ismail Trabelsi [1], Chedly Tizaoui [3,*] and Mohamed Ali Wahab [1,*]

[1] Laboratory of Wastewater Treatment and Valorization, Water Research and Technologies Center of Borj-Cedria, University of Carthage, Soliman 8020, Tunisia; amani.haddouk92@gmail.com (A.H.); ismail.trabelsi@certe.rnrt.tn (I.T.)
[2] Faculty of Sciences of Bizerte, University of Carthage, Jarzouna, Bizerte 7021, Tunisia
[3] Water and Resources Recovery Research Laboratory, Department of Chemical Engineering, Swansea University, Bay Campus, Fabian Way, Swansea SA1 8EN, UK
* Correspondence: c.tizaoui@swansea.ac.uk (C.T.); mohamedali.wahab@certe.rnrt.tn (M.A.W.)

Abstract

Excess nutrients in wastewater pose significant environmental risks, highlighting the need for low-cost treatment strategies that enable their removal. This study evaluated the adsorption capacity of woodchip biochar, a widely available waste material, for phosphate (PO_4^{3-}), nitrate (NO_3^-), and ammonium (NH_4^+) in raw and secondary-treated wastewater, and compared the results against those obtained using synthetic solutions. Approach to equilibrium was reached quicker for NH_4^+ (≈20 min) than for NO_3^- and PO_4^{3-} (≈40 min), with NH_4^+ removal reaching up to 80% at a dosage of 20 g/L. Nutrient adsorption kinetics were best described by the pseudo-second-order model for the anionic species (NO_3^- and PO_4^{3-}), while the pseudo-first-order model provided a better fit for the cationic species NH_4^+. The Freundlich isotherm provided a good fit to the equilibrium data for all species, indicating the presence of heterogeneous adsorption sites. SEM–EDX and FTIR analyses confirmed nutrient adsorption onto the biochar surface and highlighted the involvement of carboxyl and hydroxyl functional groups, with FTIR showing the greatest spectral changes for NH_4^+. Adsorption tests using secondary-treated wastewater showed high removal efficiencies (100% PO_4^{3-}, 25.4% NO_3^-, 89.5% NH_4^+), whereas performance in raw wastewater was poor (maximum 32% NH_4^+). Overall, woodchip biochar demonstrates strong potential as a tertiary treatment material, and its nutrient-saturated form may be reused as fertiliser, supporting nutrient recovery within a circular-economy framework.

Keywords: woodchips biochar; adsorption; nutrients; wastewater; sustainability; environment

Academic Editor: Alessandro Erto

Received: 4 December 2025
Revised: 28 December 2025
Accepted: 8 January 2026
Published: 13 January 2026

1. Introduction

Nitrogen (N) and phosphorus (P) are essential nutrients that play vital roles in the structure, metabolism, and overall functioning of living organisms. For instance, N is a key component of amino acids and proteins, while P is essential for genetic material, cell membranes, and energy transfer processes [1]. However, excessive amounts of N and P discharged into the aquatic environment pose a significant environmental concern due to their role in driving eutrophication, which can lead to harmful algal blooms, impacting the ecosystem and human health [2]. To protect the environment, strict regulations governing nutrient discharges have been implemented worldwide. For example, in Tunisia, where this study was conducted, wastewater discharges into natural and public hydraulic environments are regulated under Standard NT 106.02 [3], which aims to control eutrophication.

According to this standard, the maximum allowable concentrations for discharge into the public hydraulic domain are 2 mg P/L for total phosphorus, 10 mg N/L for ammoniacal nitrogen, and 50 mg/L for nitrate (NO_3^-). Meeting these limits often requires advanced or tertiary treatment processes beyond conventional secondary wastewater treatment.

Domestic sewage, often rich in these nutrients, present a major contributor to nutrient loading in water bodies. In agricultural regions, the overuse of chemical fertilisers and pesticides also accelerates nutrient runoff into surrounding watercourses. Additionally, livestock manure and aquaculture feed inputs further contribute to nutrient accumulation. These anthropogenic activities collectively intensify water eutrophication, leading to ecosystem degradation, biodiversity loss, algal blooms, fish mortality, and significant economic impacts [4,5]. Therefore, efficient, economical, and environmentally friendly technologies for N and P removal are crucial to mitigate nutrient pollution and preserve the aquatic ecosystem.

In aquatic environments, inorganic nitrogen and phosphorus primarily occur as ammonium (NH_4^+), nitrate (NO_3^-), and phosphate (PO_4^{3-}) ions [4]. Various physical, chemical, and biological treatment processes have been employed to control these pollutants, including biological nutrient removal, chemical precipitation, and advanced membrane technologies. However, these conventional approaches are often energy-intensive, operationally complex, and costly, and they typically convert nutrients to gaseous forms or generate sludge, limiting their potential for reuse. For instance, biological nitrification-denitrification, a widely applied approach for nitrogen removal in conventional wastewater treatment plants, requires strict control of operational parameters such as dissolved oxygen, temperature, pH, and sludge age, as well as sufficient internal or external carbon sources for denitrification [6,7]. It is also energy-intensive and demands skilled operation, which can limit its applicability in small-scale, decentralised, or resource-limited systems. Moreover, achieving increasingly stringent effluent discharge limits often necessitates additional tertiary treatment for nitrogen. On the other hand, while chemical precipitation is commonly employed for phosphorus removal, it can also result in excessive sludge production, increased chemical consumption, and higher operational costs [7,8]. Alternative technologies such as ion exchange, membrane filtration, and advanced oxidation processes can deliver high nutrient removal efficiencies, but they also have drawbacks such as high capital and operating costs, membrane fouling, and complex operation and maintenance requirements [9–11]. The differing ionic charges of nutrient species, cationic ammonium and anionic nitrate and phosphate often necessitate selective membranes or multiple treatment units, further increasing system complexity and cost.

As a result, low-cost tertiary treatment methods, particularly adsorption-based processes, have gained attention due to their simplicity, flexibility, and effectiveness [12,13]. The use of natural or waste-derived adsorbents is especially promising because these materials are often abundant, renewable, and inexpensive, contributing to resource recovery and circular economy objectives. Among these, biochar has emerged as a highly effective adsorbent due to its available surface area, porous structure, and versatile surface chemistry, which enable the retention of N and P nutrients [14]. Its ability to recover nutrients in plant-available forms further enables the beneficial reuse of nutrient-loaded biochar as a soil amendment or fertiliser, thereby supporting nutrient recycling and circular economy principles. Thus, this approach offers broader environmental benefits by reducing reliance on synthetic fertilisers, lowering associated greenhouse gas emissions, and by mitigating surface- and groundwater pollution and eutrophication.

Biochar, which is a carbon-rich material, is produced by the thermochemical conversion of biomass under limited oxygen (O_2) conditions, typically at temperatures ranging from 200 to 900 °C [4,15]. Common feedstock materials include agricultural and forestry

residues, animal waste, food processing byproducts, paper mill waste, municipal solid waste, and sewage sludge [16,17]. Owing to its high carbon content, surface area, ion-exchange capacity, and pH buffering ability, biochar exhibits strong adsorption potential for various pollutants [14]. Consequently, biochar has attracted attention as a multifunctional material for environmental remediation, demonstrating effectiveness in the removal of inorganic nutrients such as NH_4^+, NO_3^- and PO_4^{3-}, as well as organic contaminants (e.g., sulfamethoxazole, phenanthrenes, pesticides) and heavy metals (e.g., Pb, Cu, Cd) from wastewater [14].

Although numerous studies have demonstrated the potential of biochar for nutrient removal, several limitations remain in the existing literature. Most studies have relied on synthetic nutrient solutions, and in many cases the focus has been limited to the adsorption of single contaminants, rather than more complex mixtures and realistic wastewater matrices. While these studies have provided valuable insights into adsorption mechanisms, they do not accurately represent the complexity of real wastewaters, which contain competing ions and organic matter that can significantly affect adsorption efficiency. Furthermore, the adequate stage at which biochar adsorption should be applied within the wastewater treatment process remains poorly understood. In particular, it is unclear whether biochar adsorption is more effective when implemented at an early stage for crude sewage or after biological treatment.

In this context, the present study investigates a biochar produced from locally available woodchip waste in Tunisia and evaluates its performance for the simultaneous removal of phosphorus and nitrogen from mixed nutrient systems using both raw and secondary-treated real wastewater. Specifically, the novelty and significance of this study include (1) the valorisation of locally available woodchip waste into a low-cost and sustainable biochar adsorbent, supporting circular economy principles, (2) the demonstration of effective simultaneous adsorption of three nutrient species with distinct chemical characteristics (anionic phosphate and nitrate, and cationic ammonia), and (3) the achievement of appreciable adsorption capacities without any chemical or physical modification of the biochar, reducing treatment complexity and costs.

The biochar was produced by pyrolysis at approximately 550 °C without further treatment or functionalisation. The study presents a detailed characterisation of both the biochar and the wastewater matrices used. It identifies the adsorption isotherms and kinetic models that best describe the mechanisms governing nitrogen and phosphorus removal by the woodchip biochar and compares adsorption performance between real and synthetic wastewater. Overall, the findings provide valuable insights into the practical applicability of a wood-based biochar for nutrient removal from real wastewater matrices. Beyond demonstrating effective nutrient removal, the study highlights the potential of this approach to enable resource recovery and waste valorisation by transforming locally available wood waste into a low-cost adsorbent. It also supports the potential for beneficial reuse of nutrient-loaded biochar as a soil amendment or slow-release fertiliser, further enhancing the environmental sustainability of the approach.

2. Materials and Methods

2.1. Biochar Preparation

Woodchips were used as the feedstock material for biochar production. The pyrolysis experiments were conducted in a tubular furnace reactor. The ground biomass was placed in a quartz boat, which was then inserted into the reactor. The furnace was programmed to heat up to 550 °C at a rate of 10 °C/min under a continuous nitrogen (N_2) atmosphere to ensure an O_2-free environment. After the system cooled to room temperature, the

resulting biochar was collected, ground, and stored in airtight containers for further use. The obtained biochar samples were denoted as BW for woodchip-derived biochar.

2.2. Biochar Characterisation

The biochar samples were characterised for their elemental composition (C, H, N, and S) using a CHNS analyser (LECO CHNS-932, MI, USA). Proximate analysis, including the determination of moisture, ash, volatile matter (VM), and fixed carbon (FC), was performed with a Discovery SDT 650 thermogravimetric analyser (TG 209 F3, Netzsch, Delaware, USA) following ASTM D7582 [18]. Metal content was analysed using inductively coupled plasma atomic emission spectroscopy (ICP-OES, Elan 6000 Sciex, Perkin Elmer, CT, USA). The morphology of the biochar samples before adsorption was examined using a scanning electron microscope (SEM, Hitachi S-3000N, Japan). Samples were gold-coated with a Sputter Coater SC502 prior to imaging. Micrographs were captured under high vacuum at an accelerating voltage of 15 kV using secondary and backscattered electron detectors. After adsorption, the surface morphology of biochar was further analysed using an Thermo Fisher Scientific FEI Quanta 250 SEM, USA operating at 20 kV. The pH values of the biochar and virgin woodchip were measured using a pH metre in an aqueous suspension of 1 g biochar (or woodchip) in 10 mL of deionised water after stirring overnight. Fourier transform infrared spectroscopy (FTIR) analyses were conducted to identify the main surface functional groups of BW before and after adsorption. Approximately 0.1 g of biochar was finely ground with 1 g of spectroscopic-grade KBr, and the resulting mixture was pressed into pellets for measurement.

2.3. Aqueous Solutions Preparation and Analysis

Synthetic solutions of NH_4^+, PO_4^{3-}, and NO_3^- were prepared by dissolving analytical-grade ammonium chloride (NH_4Cl), potassium dihydrogen phosphate or monopotassium phosphate (KH_2PO_4), and potassium nitrate (KNO_3), respectively, in distilled water. These solutions served as the sources of NH_4^+, PO_4^{3-}, and NO_3^- ions for the adsorption experiments. Their concentrations were measured using a Metrohm 940 Professional ion chromatograph equipped with a conductivity detector, Herisau, Switzerland. The injection flow rate was set at 0.7 mL/min. For anions, the eluent consisted of 1.8 mM sodium carbonate (Na_2CO_3) and 1.7 mM sodium bicarbonate ($NaHCO_3$). For cations, a mixture of 1 mol/L nitric acid and dipicolinic acid was used. A self-regenerating suppressor (SRS) with a suppression current of 30 mA was used to enhance the conductivity of the analytes. The system was equipped with an anion-exchange column (AS4A-SC, 150 mm × 4 mm, Herisau, Switzerland) and a cation-exchange column (AS4A-SC, 150 mm × 4 mm), and the data were processed using IC NET software (version 2.3).

2.4. Batch Adsorption Studies

Batch adsorption experiments were carried out to investigate the effects of various operational parameters, including initial ion concentration, contact time, solution pH, and adsorbent dosage, on the removal of NH_4^+, NO_3^- and PO_4^{3-} by BW. All experiments were performed at 25 °C. In each assay, a known mass (varied between 2 and 20 g/L) of biochar was added to 100 mL of nutrient solution and agitated at 150 rpm for 120 min at 25 °C using a Biobase bio-industry (Shandong Co., Ltd., Jinan, China) thermostatic refrigerated shaker incubator (model BJPX-103B).

2.4.1. Effect of Initial Concentration and Contact Time

Five initial nutrient concentrations (10, 30, 50, 80, and 100 mg/L) were used, and adsorption was monitored at seven contact times (5, 10, 20, 40, 60, 90, and 120 min). The adsorbent dosage and solution pH were maintained at 2 g/L (dry basis) and pH 7, respectively.

2.4.2. Effect of Initial Solution pH

The influence of initial solution pH on the adsorption of NH_4^+, NO_3^- and PO_4^{3-} was evaluated by varying pH values from 2 to 11. During these experiments, the initial nutrient concentration and adsorbent dosage were fixed at 50 mg/L and 2 g/L, respectively. The solution pH was adjusted using 0.1 M HCl or 0.1 M NaOH.

2.4.3. Effect of Adsorbent Dosage

The effect of adsorbent dosage on nutrient removal efficiency was studied using a fixed initial nutrient concentration of 50 mg/L at pH 7, with agitation using a shaker at 150 rpm for 120 min. The dose of BW varied between 2 and 20 g/L.

2.4.4. Nutrient Removal Calculation

The amount of NH_4^+, NO_3^- and PO_4^{3-} adsorbed on the biochar was determined from the decrease in nutrient concentration in the aqueous solutions. At a given time t, the adsorption capacity, Q_t (mg/g), was calculated as:

$$Q_t = \frac{C_0 - C_t}{M_s} V$$

where

C_0 (mg/L) is the initial nutrient concentration;
C_t (mg/L) is the nutrient concentration at time t;
V (L) is the volume of the aqueous solution;
M_s (g) is the mass of biochar used.
The adsorption removal efficiency (R, %) at time t was calculated using:

$$R = 100 \frac{C_0 - C_t}{C_0}$$

2.5. Modelling Studies

2.5.1. Kinetic Models

In adsorption studies, several kinetic models are commonly employed to describe the rate of solute uptake. Among these, the most widely used are the pseudo-first-order and pseudo-second-order models (Table 1). In this study, these kinetic models were applied to evaluate the adsorption behaviour of NH_4^+, NO_3^- and PO_4^{3-} on BW. Model parameters were obtained by fitting experimental data using Excel Solver (Version 2512), minimising the sum of squared differences between the measured and calculated values.

Table 1. Adsorption kinetic models.

Model	Equation	Model Parameters
Pseudo-first-order	$Q_t = Q_e(1 - \exp(-K_1 t))$	Q_e, K_1
Pseudo-second-order	$Q_t = \frac{K_2 Q_e^2 t}{1 + K_2 Q_e t}$	Q_e, K_2

2.5.2. Adsorption Isotherms

Adsorption isotherms describe the equilibrium relationship between the amount of solute adsorbed on a solid surface and its concentration in the solution at a constant temperature. In this study, the equilibrium adsorption data for PO_4^{3-}, NO_3^-, and NH_4^+ on BW were analysed using the Freundlich, Langmuir, and Temkin isotherm models (Table 2). These models provide insights into the adsorption capacity, surface heterogeneity, and interaction energies. The model parameters were obtained by fitting experimental data

using Excel Solver (Version 2512), minimising the sum of squared differences between the measured and calculated values.

Table 2. Adsorption isotherm models.

Isotherm	Equation	Model Parameters
Langmuir	$Q_e = Q_m \frac{K_L C_e}{1+K_L C_e}$	Q_m, K_L
Freundlich	$Q_e = K_F C_e^{\frac{1}{n}}$	K_F, n
Temkin	$Q_e = \frac{RT}{B_T} Ln(A_T C_e)$	B_T, A_T

2.6. Biochar Testing for Real Wastewater Treatment

Samples of raw and secondary-treated urban wastewater were collected from the Grombalia Wastewater Treatment Plant (WWTP) in Tunisia (Figure 1) and stored at 4 °C in dark until use. The physicochemical characteristics of the raw and secondary-treated wastewater used in this study are presented in Table 3, with the concentrations of the nutrients (PO_4^{3-}, NO_3^-, and NH_4^+) highlighted in bold.

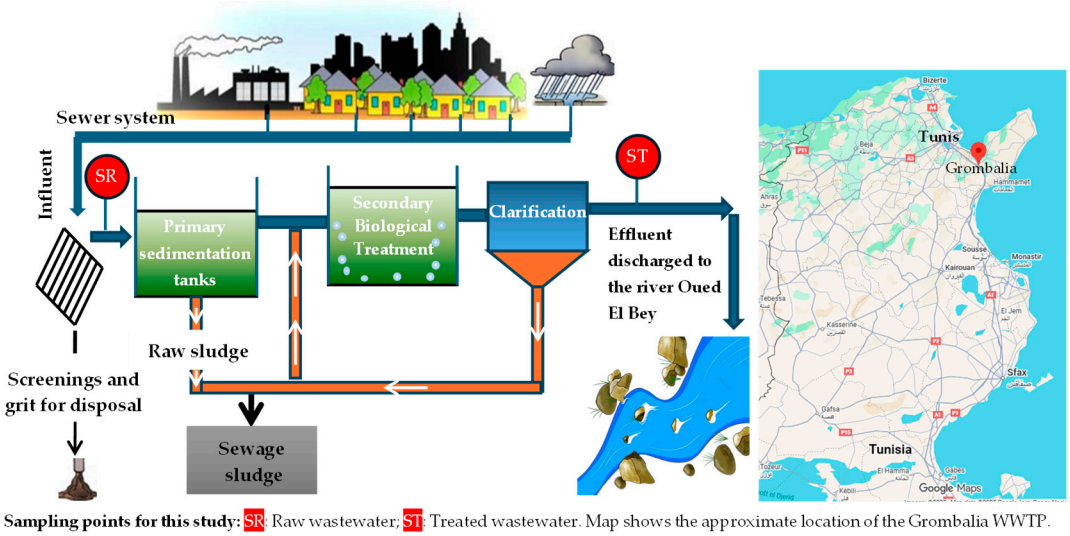

Figure 1. Key processes of the Grombalia WWTP.

Table 3. Physicochemical characteristics of raw and secondary-treated wastewater.

Parameters	Raw Wastewater	Treated Wastewater
pH	7.58	8
EC (mS/cm)	1846	2340
COD (mg/L)	230.4	96
SS (mg/L)	145	3
Cl^- (mg/L)	398.52	400.02
Br^- (mg/L)	7.17	5.90
NO_3^- (mg/L)	**7.12**	**97.25**
SO_4^{2-} (mg/L)	294.90	325.33
PO_4^{3-} (mg/L)	**13.38**	**9.32**
Na^+ (mg/L)	191.91	165.52
NH_4^+ (mg/L)	**73.96**	**2.06**
K^+ (mg/L)	22.24	32.66
Ca^{2+} (mg/L)	88.27	77.57
Mg^{2+} (mg/L)	22.32	23.97

Note: Nutrients used in this study are indicated in bold.

Batch experiments were performed by contacting 100 mL of wastewater with 0.2 g of biochar (equivalent to an adsorbent dose of 2 g/L) under agitation using a shaker at 150 rpm for 120 min. At the end of the contact period, the solutions were filtered through 0.45 µm filter paper and analysed for nutrient by ion chromatography.

The Grombalia WWTP (Figure 1) uses a conventional activated sludge process with a low organic loading rate to treat urban wastewater. Influent wastewater first undergoes preliminary treatment, including screening and grit removal, to eliminate coarse solids and inert materials followed by sedimentation tanks for primary treatment. The effluent then enters aeration basins, where organic matter is degraded by microorganisms in the presence of a supply of air. The mixed liquor then flows to secondary clarifiers, where the activated sludge is separated by sedimentation. Some of the settled sludge is recirculated to maintain sufficient biomass in the aeration tanks, while excess sludge is removed for further treatment. Finally, the treated effluent is discharged into a nearby river (Oued El Bey) in compliance with national discharge standards.

3. Results and Discussion

3.1. Characterisation of the Biochar

The physicochemical properties of the raw woodchips and the produced biochar (BW) are summarised in Table 4. The biochar exhibited a significantly higher pH (9.7) compared to the raw woodchips, reflecting the formation of alkaline functional groups during pyrolysis as also found in other studies [19].

Table 4. Physicochemical properties of biochar.

Sample	pH	Proximate Analysis			Elemental Analysis (%)				
		VM	Ash	FC	C	H	N	S	O_2
Woodchips	6.7	62.7	36.5	0.8	38.5	5.2	1.3	0.22	54.7
BW	9.7	17.0	10.6	72.4	75.97	2.65	0.85	0.1	20.43

Proximate analysis showed a marked decrease in VM from 62.7% in woodchips to 17.0% in BW, while FC increased from 0.8% to 72.4%, indicating enhanced carbonisation and the formation of a more stable, carbon-rich matrix. The ash content decreased from 36.5% to 10.6%, suggesting the partial loss of inorganic components during pyrolysis.

Elemental analysis revealed a substantial increase in carbon content from 38.5% in the raw material to 75.97% in BW, whereas hydrogen and nitrogen contents decreased, consistent with the loss of labile organic compounds and VM. Sulphur content decreased slightly (0.22% to 0.1%), while O_2 content dropped from 54.7% to 20.43%, confirming the enrichment of carbon and the reduction of oxygenated functional groups.

3.2. Batch Experiments

3.2.1. Effect of Initial Nutrient Concentrations and Contact Time

The results presented in Figure 2a–c clearly show that the adsorption of NH_4^+, NO_3^- and PO_4^{3-} onto the biochar is time-dependent. For NO_3^- and PO_4^{3-}, the amounts adsorbed (Q_t) increased rapidly during the first 20 min, reaching approximately 75% of the total equilibrium uptake across all initial concentrations tested. Beyond 20 min, adsorption continued to rise but at a slower rate, approaching equilibrium at about 40 min (Figure 2a,b).

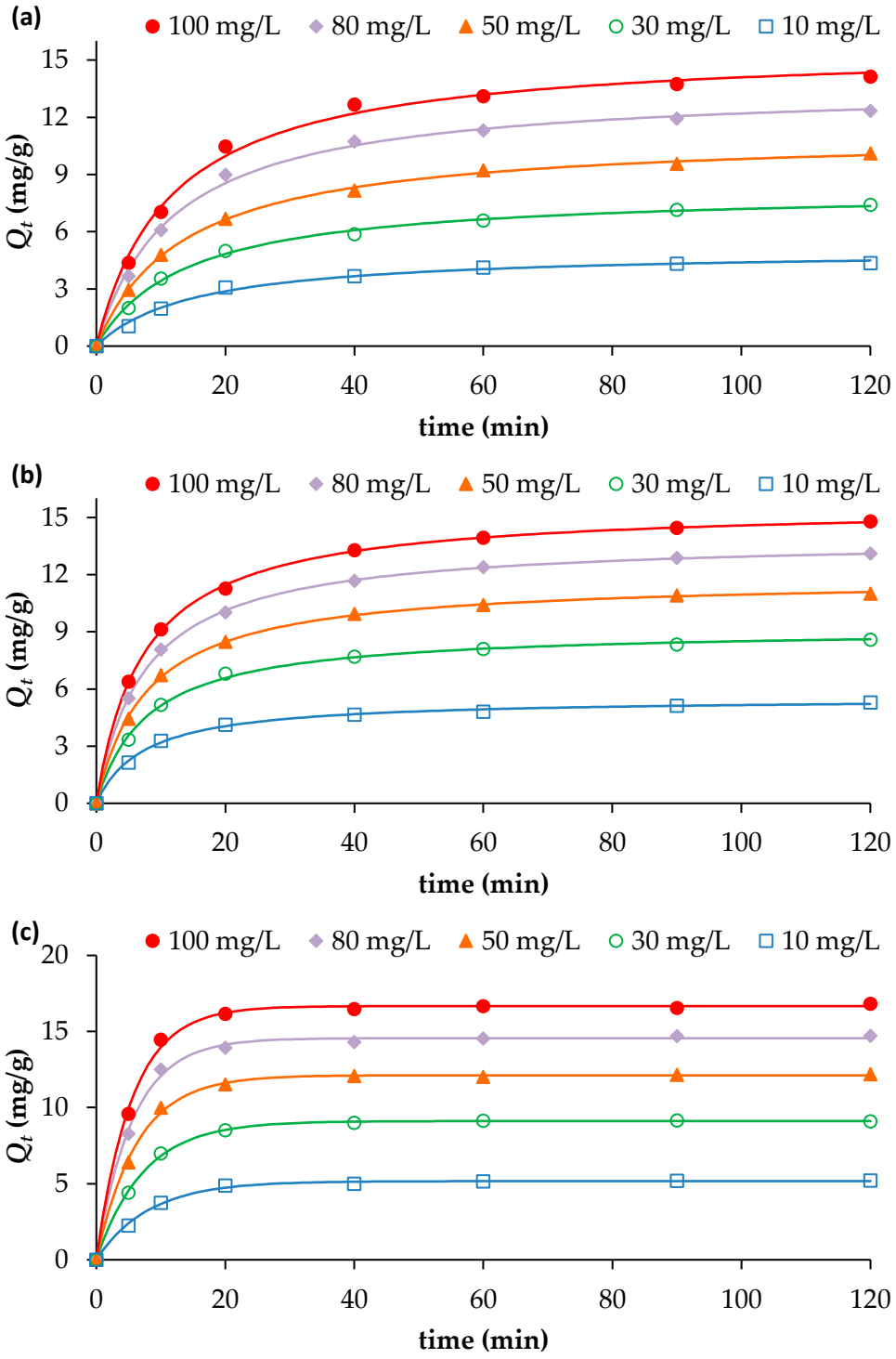

Figure 2. Effect of contact time and initial nutrient concentrations on the adsorption of (**a**) PO_4^{3-}, (**b**) NO_3^- and (**c**) NH_4^+, onto BW (adsorbent dosage = 2 g/L; pH = 7; Temperature = 25 °C). Continuous lines indicate model fitting of the experimental data (further details on Section 3.3).

For NH_4^+, the adsorption occurred even more rapidly: approximately 80% of the total uptake was achieved within the first 10 min, followed by a gradual approach to equilibrium at 20 min (Figure 2c). This rapid initial phase can be attributed to the abundance of available adsorption sites and a strong concentration gradient between the liquid and solid phases [14]. The subsequent slowdown in adsorption kinetics for all three nutrients is due to the progressive occupation of active sites and reduction in concentration gradient,

leading to reduced mass transfer and possible electrostatic repulsion between adsorbed species and the biochar surface [20].

An increase in initial nutrient concentration also enhanced the adsorption capacity of the biochar. Raising the initial concentration from 10 to 100 mg/L increased the adsorption capacities (measured at the maximum time 120 min) from 4.36 to 14.13 mg/g for PO_4^{3-}, from 5.29 to 14.80 mg/g for NO_3^-, and from 5.20 to 16.83 mg/g for NH_4^+. As the initial solute concentration increases, the driving force for mass transfer between the solution and the adsorbent surface also increases. This stronger concentration gradient promotes greater diffusion of solute molecules toward the adsorption sites, resulting in a higher adsorption capacity.

Compared with other biochars reported in the literature, BW exhibited notably higher adsorption performance, particularly for NH_4^+. For example, a giant reed-derived biochar produced at 500 °C achieved only 1.805 mg/g [21], while other plant-based biochars pyrolysed at 500 °C reported comparable capacities to our study up to 13.35 mg/g [22]. For NO_3^-, the adsorption capacity of BW exceeded that of wheat straw biochar pyrolysed at 450 °C (2.47 mg/g) [23], though it remained lower than that of oak sawdust biochar produced at 600 °C [24]. For PO_4^{3-}, BW exhibited higher adsorption capacities than those reported for corn biochar pyrolysed at 500 °C, which exhibited only 0.036 mg/g, and peanut shell biochar produced at 700 °C with a capacity of 7.56 mg/g [25,26]. These differences in nutrient uptakes could be explained by differences in feedstock chemistry, pyrolysis conditions, mineral content, functional groups, surface area, and experimental setups. Each factor shapes the biochar's physicochemical properties and, therefore, its affinity for these nutrients.

3.2.2. Effect of Aqueous Initial pH

The influence of solution pH on the adsorption of PO_4^{3-}, NO_3^- and NH_4^+ by BW is illustrated in Figure 3. The results show that pH has a significant impact on nutrient adsorption behaviour, mainly due to variations in the adsorbent surface charge and the ionic speciation of the adsorbates [27].

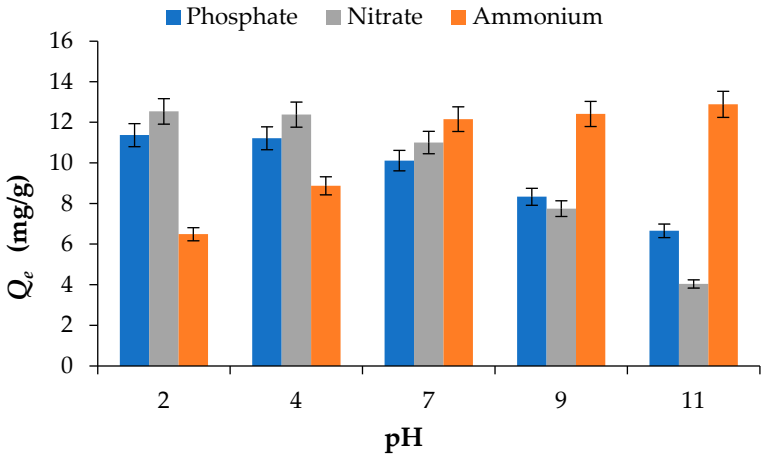

Figure 3. Effect of pH on the adsorption of phosphate PO_4^{3-}, nitrate NO_3^- and ammonium NH_4^+ onto BW (adsorbent dosage = 2 g/L; initial concentration = 50 mg/L; Temperature = 25 °C).

For PO_4^{3-} and NO_3^-, the adsorption capacity, taken as the uptake at 120 min, decreased with increasing pH, showing maximum uptake under acidic conditions. At a constant initial concentration of 50 mg/L, the adsorption capacities of PO_4^{3-} and NO_3^- were 6.65 mg/g and 4.04 mg/g, respectively, at pH 11, increasing to 11.37 mg/g and 12.54 mg/g at pH 2. The higher adsorption observed under acidic conditions has also been reported by [28] and can be attributed to protonation of the biochar surface, which enhances

electrostatic attraction between the biochar surface and the negatively charged PO_4^{3-} and NO_3^-. As pH increases, deprotonation of functional groups such as –COOH and –OH occurs, resulting in the development of negative surface charges that electrostatically repel anions and consequently reduce adsorption efficiency [14].

In contrast, NH_4^+ adsorption showed the opposite trend, increasing as pH rose from 2 to 7. For example, the adsorption capacity increased from 6.49 mg/g at pH 2 to 12.16 mg/g at pH 7. Increasing the pH above 7 resulted in only marginal increase in adsorption capacity, reaching 12.41 mg/g at pH 9 and 12.89 mg/g at pH 11. This enhanced uptake at neutral to alkaline pH can be explained by the decreased competition from H^+ ions for adsorption sites and the predominance of electrostatic attraction between negatively charged biochar surfaces and NH_4^+ cations [27–29].

3.2.3. Effect of Adsorbent Dosage

The effect of biochar dosage on the removal efficiency of nutrient ions is presented in Figure 4. Overall, the results show that the removal efficiency increased with increasing adsorbent dosage. For phosphorus, the removal efficiency increased from 39.7% to 70.8% as the biochar dose was raised from 2 g/L to 20 g/L. Similarly, for NO_3^-, the removal efficiency reached approximately 74% at the highest dosage of 20 g/L. The most pronounced effect was observed for NH_4^+, where the initial concentration of approximately 50 mg/L decreased to 28 mg/L at a biochar dose of 2 g/L and further to 10 mg/L at a dose of 20 g/L, corresponding to a removal efficiency of about 80%. This improvement with higher adsorbent dosage can be attributed to the increased number of available active sites and the larger surface area available for nutrient adsorption, which enhance the overall removal performance [12].

The nutrient removal efficiencies observed in this study are consistent with trends reported in the literature for biochar systems at varying dosages. NH_4^+ removal reached 80% at 20 g/L, comparable to unmodified biochars, which typically show NH_4^+ adsorption capacities below 20 mg/g [1]. Previous studies [24–30] also reported that increasing biochar dosage enhances overall removal efficiency while reducing unit adsorption capacity, supporting the trends observed here. PO_4^{3-} removal of 70.8% at 20 g/L exceeds values reported for several unmodified biochars, such as 38.1% by [22]. Notably, NO_3^- removal reached 74% at 20 g/L, substantially higher than that of most unmodified biochars, which generally exhibit very low NO_3^- sorption [1].

Although the removal efficiency increased with increasing adsorbent dose, the uptake capacity of the biochar decreased as the dose increased (Figure 4). This trend is consistent with the fundamental uptake equation, in which the adsorption capacity is inversely proportional to the adsorbent dose ($Q = (C_0 - C_f)/D$), where Q is the uptake capacity (mg/g), D is the adsorbent dose (g/L), and C_0 and C_f are the initial and final solute concentrations (mg/L)), respectively. However, as shown in Figure 4, the experimentally measured uptake was consistently lower than the uptake expected at equilibrium, as predicted from the adsorption isotherm determined at a dose of 2 g/L (Section 3.4). The discrepancy between the expected ($Q_{expected}$) and measured ($Q_{measured}$) uptake ranged from 26 to 34% for phosphate, 25–30% for nitrate, and 19–27% for ammonium. This deviation from equilibrium adsorption capacity may be attributed to particle agglomeration or overlapping of adsorption sites at higher adsorbent doses, which reduces the effective surface area available for adsorption and increases diffusion path lengths, thereby lowering uptake per unit mass [31]. Reviews of biomass-derived adsorbents note that at excessive biochar or activated carbon dosages, adsorption layers may overlap and active sites become less accessible, diminishing adsorption efficiency per unit adsorbent [32]. Together these studies support the assertion that agglomeration and reduced surface site accessibility at

higher adsorbent doses can cause measured uptake to fall below expected equilibrium capacities. This highlights the importance of optimising the adsorbent dose to balance maximising uptake per unit mass with the effective amount of material applied per unit volume of wastewater.

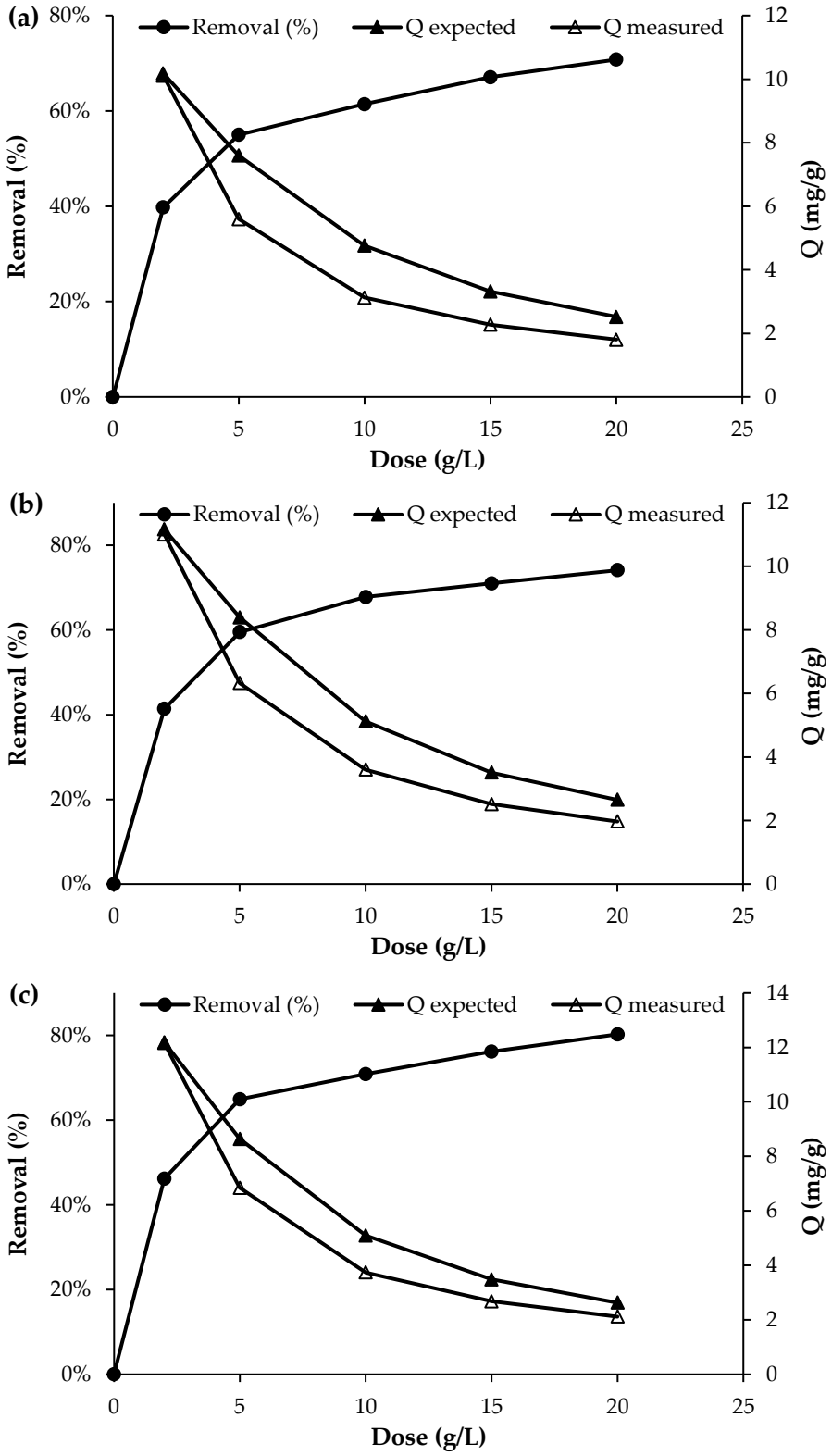

Figure 4. Effect of adsorbent dosage on the adsorption of (**a**) PO_4^{3-}, (**b**) NO_3^- and (**c**) NH_4^+ (initial concentration = 50 mg/L; pH = 7; T = 25 °C; contact time = 120 min).

3.3. Adsorption Kinetic Modelling

The fitted parameters for the pseudo-first-order and pseudo-second-order kinetic models are presented in Table 5. As shown, both models describe the adsorption kinetics reasonably well; however, the pseudo-second-order model provides a markedly better fit for anionic species (PO_4^{3-} and NO_3^-), whereas the pseudo-first-order model is more appropriate for the cationic species NH_4^+. The experimentally measured adsorption capacities at 120 min align closely with the equilibrium capacities predicted by the respective kinetic models, further validating the reliability of the model fits. Table 5 also indicates that the initial concentration has only a minor influence on the pseudo-first-order rate constant (k_1). In contrast, the pseudo-second-order rate constant (k_2) is strongly affected by the initial concentration, showing a decreasing trend as the initial concentration increases. This suggests that higher solute concentrations progressively slow the rate of adsorption. A review of theoretical and experimental adsorption kinetics points out that k_2 is often a decreasing function of the initial concentration (C_0), because k_2 is effectively a time-scaling factor: higher initial concentrations typically require longer times to reach equilibrium [33].

Table 5. Kinetic rate constants of nutrients adsorption onto BW at different initial concentrations.

			Pseudo-First-Order Model			Pseudo-Second-Order Model		
Nutrients	**C_0 (mg/L)**	**Experimental Q_e (mg/g)**	**k_1 (min^{-1})**	**Calculated Q_e (mg/g)**	**R^2**	**k_2 (g.mg/min)**	**Calculated Q_e (mg/g)**	**R^2**
Phosphate	10	4.4	0.059	4.3	0.996	0.013	5.1	0.994
	30	7.4	0.062	7.0	0.987	0.009	8.2	0.997
	50	10.1	0.063	9.6	0.990	0.007	11.2	0.999
	80	12.3	0.070	11.8	0.996	0.006	13.7	0.997
	100	14.1	0.072	13.7	0.997	0.006	15.7	0.996
Nitrate	10	5.3	0.103	5.0	0.989	0.025	5.5	0.998
	30	8.6	0.096	8.2	0.994	0.014	9.2	0.998
	50	11.0	0.096	10.6	0.991	0.011	11.8	1.000
	80	13.1	0.100	12.5	0.988	0.010	13.9	1.000
	100	14.8	0.101	14.1	0.987	0.009	15.6	1.000
Ammonium	10	5.2	0.124	5.2	0.997	0.032	5.6	0.982
	30	9.1	0.138	9.1	0.999	0.021	9.8	0.987
	50	12.2	0.159	12.1	0.999	0.020	13.0	0.985
	80	14.7	0.177	14.6	0.998	0.019	15.5	0.987
	100	16.8	0.182	16.7	0.998	0.018	17.7	0.984

The kinetic modelling results obtained in this study are consistent with literature observations on nutrient adsorption by biochar systems with a predominance of pseudo-second-order kinetics (R^2 = 0.982–1.000), aligning with numerous studies on nutrient removal. Ca^{2+}-modified soybean straw biochar exhibited adsorption capacities of 103.18 mg/g for NH_4^+-N and 9.75 mg/g for PO_4^{3-}-P, with experimental data corresponding to pseudo-second-order kinetics, indicating homogeneous adsorption through electrostatic attraction [34]. Similarly, $MgCl_2$-modified biochar from *Phragmites australis* demonstrated that NH_4^+ adsorption followed pseudo-second-order kinetics, while PO_4^{3-} exhibited multi-phase behaviour described by both intra-particle diffusion and pseudo-first-order models [35]. Fruit peel-derived biochar also followed pseudo-second-order kinetics for NH_4^+ adsorption, with the Langmuir isotherm successfully simulating the process [36]. Magnesium-doped biochar showed that the pseudo-second-order model accurately described adsorp-

tion of both phosphorus and ammonium nitrogen across all tested solutions [37]. The concentration-dependent decrease in k_2 values observed in this study has been documented in other biochar systems, reflecting finite availability of high-energy adsorption sites and increased competition at elevated pollutant loadings [34]. The consistency between our results (Q_e = 15.6–17.7 mg/g) and literature values for unmodified biochar further supports the reliability of the kinetic modelling approach employed in this study.

3.4. Adsorption Isotherms

The determination of adsorption equilibrium isotherms is essential for assessing the feasibility and mechanism of the adsorption process, as it provides insight into the distribution of solute molecules between the liquid and solid phases at equilibrium. In this study, adsorption isotherms for PO_4^{3-}, NO_3^-, and NH_4^+ onto BW were evaluated at 25 °C using different initial solute concentrations, while maintaining a constant adsorbent dosage of 2 g/L. The equilibrium data were analysed using three commonly applied isotherm models: Langmuir, Freundlich, and Temkin (Figure 5).

The adsorption constants obtained from the three isotherm models, together with their corresponding correlation coefficients, are presented in Table 6. Among the evaluated models, the Freundlich isotherm provided the best fit to the experimental data, exhibiting the highest regression coefficients (R^2 = 0.990–0.993). This was followed by the Langmuir model (R^2 = 0.805–0.920) and the Temkin model (R^2 = 0.830–0.877).

Table 6. Parameters of the isotherms.

Nutrient	Langmuir			Freundlich			Temkin		
	K_L (L/mg)	Q_m (mg/g)	R^2	K_F (mg·L$^{1/n}$/(g·mg$^{1/n}$))	1/n	R^2	A_T (L/mg)	B_T (kJ/mol)	R^2
Phosphate	0.074	15.6	0.917	3.20	0.339	0.993	0.403	609.2	0.869
Nitrate	0.233	13.7	0.805	4.24	0.283	0.993	0.590	647.3	0.877
Ammonium	0.073	18.9	0.920	4.23	0.316	0.990	0.426	512.1	0.830

The superior fitting of the Freundlich model indicates that nutrient adsorption onto BW occurs on a heterogeneous surface with a non-uniform distribution of active sites, and that multilayer adsorption is likely involved. This suggests that the adsorption mechanisms for PO_4^{3-}, NO_3^- and NH_4^+ on BW are better characterised by heterogeneous interactions rather than a uniform monolayer assumption, as implied by the Langmuir model. This is corroborated by the magnitude of the Freundlich exponent ($1/n$) values of 0.339, 0.283, and 0.316 for PO_4^{3-}, NO_3^- and NH_4^+, respectively, which all fall within the range of 0.1–1, implying that the adsorption of all three nutrients onto the biochar is favourable and heterogeneous in nature. Consequently, the Freundlich model provides the most reliable description of nutrient adsorption behaviour on BW under the conditions examined.

3.5. Surface Morphology and Chemical Changes of Biochar Following Nutrient Adsorption

The scanning electron microscopy (SEM) and energy-dispersive X-ray spectroscopy (EDX) analyses presented in Figure 6 and Table 7 provide comprehensive insights into the surface morphology and elemental composition changes of wood-based biochar (BW) before and after nutrient adsorption. The pristine biochar exhibits a relatively smooth surface structure with limited porosity and very low specific surface area (ABET = 0.05 m^2/g), which is consistent with the characteristics of dense carbonaceous materials produced at moderate pyrolysis temperatures. The EDX analysis of raw biochar (BW before adsorption) reveals a carbon-rich composition (75.63 atomic %), with O_2 (18.15%), minor quantities of metallic cations including Ca (1.20%), K (2.21%), Mg (0.62%), and trace phosphorus (0.89%), which play crucial roles in subsequent nutrient adsorption processes.

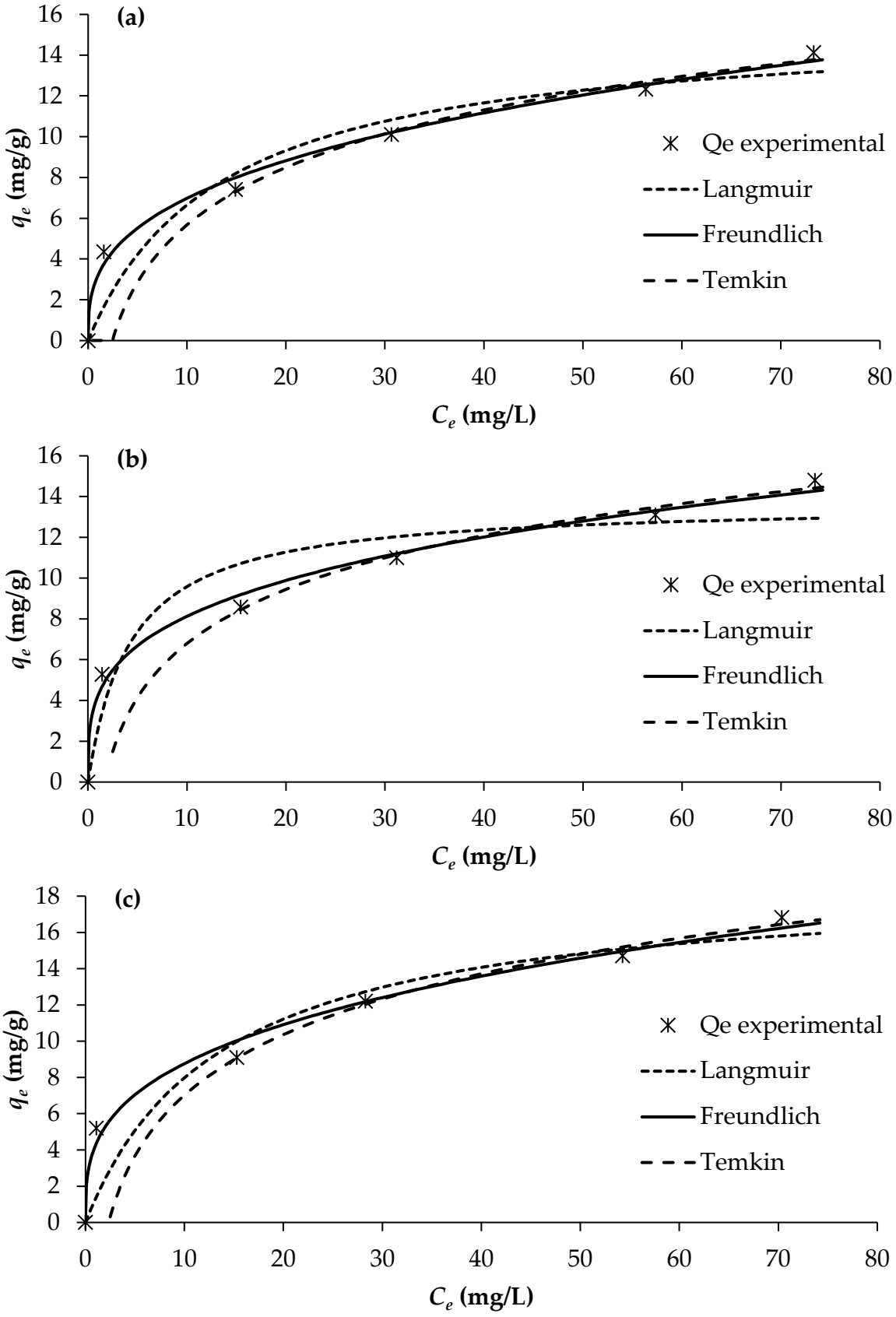

Figure 5. Adsorption isotherms of (**a**) PO_4^{3-}, (**b**) NO_3^-, and (**c**) NH_4^+ (pH = 7; temperature = 25 °C).

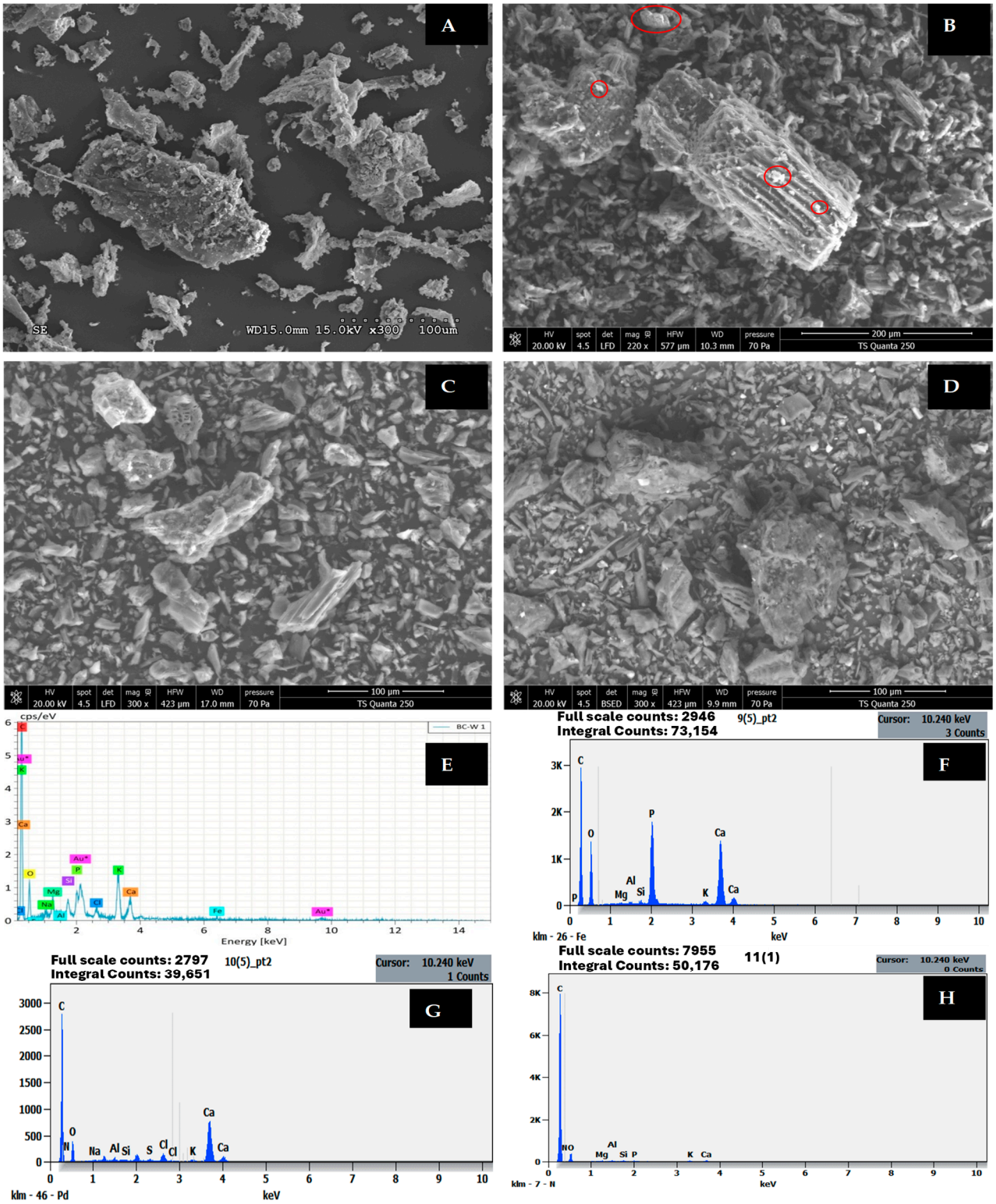

Figure 6. SEM images of BW (**A**) before adsorption, (**B**) after PO_4^{3-} adsorption, (**C**) after NH_4^+ adsorption, and (**D**) after NO_3^- adsorption. EDX of BW (**E**) before adsorption, (**F**) after PO_4^{3-} adsorption, (**G**) after NH_4^+ adsorption, and (**H**) after NO_3^- adsorption. Au*: The presence of Au is due to gold coating applied during sample preparation prior to SEM analysis.

Table 7. Quantitative results of EDX.

	Before Adsorption	After Adsorption		
		PO_4^{3-}	NH_4^+	NO_3^-
Element	**% Atomic**	**% Atomic**	**% Atomic**	**% Atomic**
C	75.63	64.41	56.70	50.88
O	18.15	26.69	18.44	24.28
N	-	-	17.48	24.10
Na	0.22	-	-	-
Mg	0.62	0.44	-	0.10
Al	0.04	3.04	0.18	0.13
Si	0.54	0.54	0.09	0.10
S	-	-	0.04	-
P	0.89	9.83	-	0.06
Cl	0.36	0.20	3.81	-
K	2.21	1.32	0.20	0.15
Ca	1.20	2.27	1.59	0.20
Fe	0.14	-	-	-

Following PO_4^{3-} adsorption, dramatic changes are observed in both surface morphology and elemental composition. The carbon content decreases significantly from 75.63% to 64.41%, while phosphorus content increases remarkably from 0.89% to 9.83% (Table 7), representing an approximately 11-fold enrichment. This substantial phosphorus accumulation is accompanied by notable increases in calcium (1.20% to 2.27%) and aluminium (0.04% to 3.04%), suggesting precipitation-based removal mechanisms. SEM-EDX analysis confirms the formation of fine spherical clusters dispersed on the surface of biochar, which were not observed before adsorption. These clusters could be formed due to precipitation of PO_4^{3-} with metals on the surface of the biochar, naturally present in biochar to form stable mineral phases such as calcium phosphate ($Ca_3(PO_4)_2$), aluminium phosphate ($AlPO_4$), and potentially magnesium phosphate $Mg_3(PO_4)_2$ compounds [38,39]. Similar morphological transformations have been documented in numerous studies where EDX mapping confirmed homogeneous distribution of Ca, Mg, and P elements on biochar surfaces after PO_4^{3-} adsorption, validating precipitation as the dominant mechanism [40,41].

The EDX analysis after NO_3^- adsorption shows intermediate characteristics with carbon content reduced to 50.88% and nitrogen content elevated to 24.10%, indicating substantial NO_3^- capture despite the expected electrostatic repulsion between NO_3^- anions and the negatively charged biochar surface. The O_2 content increases from 18.15% to 24.28%, which may reflect both adsorbed NO_3^- and increased surface oxidation during the adsorption process. The relatively high NO_3^- accumulation (24.10%) compared to NH_4^+- loading (17.48%) is noteworthy given that unmodified biochars typically exhibit minimal NO_3^- sorption capacity. This enhanced NO_3^- removal may be attributed to reduction of NO_3^- to nitrogen-containing surface functional groups [42,43]. The presence of minor quantities of Ca (0.20%), K (0.15%), and Mg (0.10%) suggests some involvement of these cations in facilitating NO_3^- retention, possibly through formation of bridge complexes.

The EDX analysis after NH_4^+- adsorption reveals distinctly different elemental patterns compared to phosphate loading. The carbon content decreases to 56.70%, while nitrogen content increases dramatically to 17.48%, providing direct evidence of successful NH_4^+- capture through ion exchange and electrostatic adsorption processes. Unlike the pronounced precipitation observed for phosphate, the nitrogen enrichment occurs without

significant changes in metallic cation concentrations, confirming that NH_4^+- adsorption proceeds primarily through cation exchange on negatively charged functional groups such as carboxyl (-COO^-) and phenolic (-OH) sites present on the biochar surface [1]. The presence of sulphur (0.04%) in the NH_4^+-loaded biochar may indicate trace adsorption of sulphate ions from the wastewater matrix. Studies on biochar modified with $MgCl_2$ have demonstrated that EDX analysis can effectively track nitrogen accumulation during NH_4^+- adsorption, with modified biochars exhibiting rougher heterogeneous surfaces and enhanced nitrogen retention compared to pristine materials [35].

Comparative analysis of the elemental composition across all four samples reveals important mechanistic insights. The carbon content follows the order pristine BW (75.63%) > PO_4^{3-}-loaded (64.41%) > NH_4^+-loaded (56.70%) > NO_3^--loaded (50.88%), indicating progressive coverage or replacement of surface carbon with adsorbed nutrient species. Studies on metal-modified biochars have shown that EDX mapping can effectively visualise the distribution of elements after adsorption, with phosphate-loaded biochars displaying clustered flake structures rich in O, Mg, and P, confirming formation of magnesium phosphate precipitates such as $MgHPO_4$ and $Mg(H_2PO_4)_2$ [40].

The EDX results obtained in this study validate that wood-based biochar achieves substantial nutrient removal through precipitation and ion exchange mechanisms, with the elemental composition changes providing quantitative evidence for the adsorption processes elucidated through kinetic and isotherm modelling.

The FTIR spectra of BW before and after nutrient adsorption are presented in Figure 7. A total of 54 infrared transmission peaks were recorded, reflecting the complex chemical composition of the biochar.

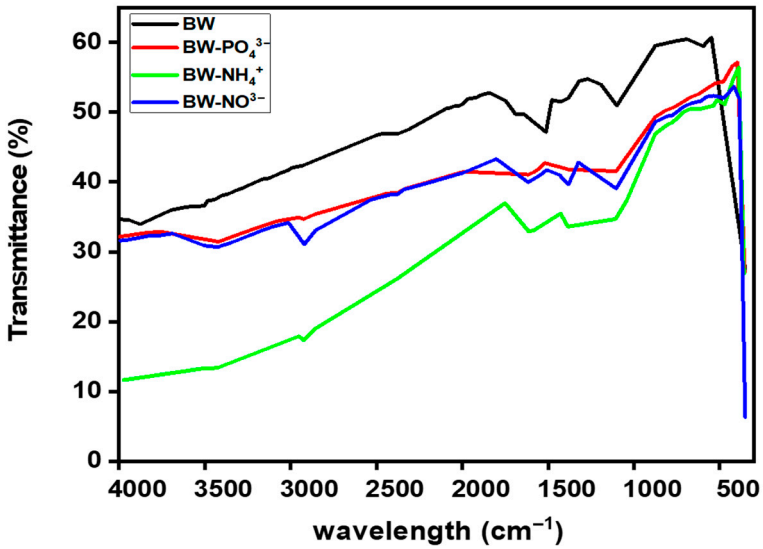

Figure 7. FTIR spectrum before and after nutrients adsorption.

Wood-derived biochar typically exhibits several characteristic bands: a broad O–H stretching vibration (≈3600–3200 cm^{-1}), weak aliphatic C–H stretching (≈2925 and 2850 cm^{-1}), carbonyl C=O stretching (≈1710–1680 cm^{-1}), aromatic C=C skeletal vibrations (≈1600–1510 cm^{-1}), and strong C–O stretching in the 1250–1000 cm^{-1} range, associated with alcohol, ether, and phenolic groups. These assignments align with previous FTIR studies on biochars produced at similar pyrolysis temperatures [44].

Following NH_4^+ adsorption (BW–NH_4^+), only 29 peaks were detected compared to 54 in the pristine biochar, indicating substantial chemical changes on the biochar surface. A diagnostic NH_4^+ deformation band appeared in the 1470–1400 cm^{-1} range, while subtle variations were observed near 3200–3300 cm^{-1}, corresponding to N–H stretching and

H-bonded O–H vibrations. These changes suggest that O_2-containing functional groups, such as hydroxyl and carboxyl groups, participated in hydrogen bonding, proton exchange, or ligand interactions with NH_4^+ ions. Minor decreases or shifts in the C=O and O–H regions further support this interaction. Overall, the loss of peaks and the observed spectral shifts confirm the strong adsorption of NH_4^+- and explain the higher adsorption capacity recorded for NH_4^+ among the three nutrients, highlighting the biochar's preferential affinity for cationic species. In situ ATR-FTIR studies on pinewood biochar have shown similar NH_4^+-related shifts, consistent with adsorption onto oxygenated functional sites under neutral to alkaline conditions [45–47].

After phosphate adsorption (BW–PO_4^{3-}), new or intensified peaks emerged in the 1100–1040 cm^{-1} region, corresponding to P–O and/or P–O–C vibrations. Weak bands also appeared around 650–500 cm^{-1}, attributable to P–O bending or metal–O–P vibrations. Concurrently, the broad O–H band became less pronounced, suggesting hydrogen bonding or ligand exchange between phosphate ions and surface hydroxyl/carboxyl groups. Moreover, of the 54 peaks observed in pristine BW, only 35 were detected after phosphate adsorption, indicating significant changes in surface chemistry. Such spectral modifications are widely reported for phosphate retention on biochars [48,49].

After NO_3^- adsorption (BW–NO_3^-), the asymmetric stretching vibration of NO_3^- appeared sharply at ~1384 cm^{-1}, accompanied by an additional out-of-plane mode near 823 cm^{-1}. The reduction in O–H band intensity suggests hydrogen bonding or outer-sphere complexation between NO_3^- ions and surface hydroxyl groups. These spectral signatures are consistent with previous reports on NO_3^- retention by (nano)biochars and related carbonaceous sorbents [50].

3.6. Biochar Testing for Real Wastewater Treatment

To evaluate the performance of BW in real wastewater, adsorption experiments were conducted using raw and secondary-treated effluent from the Grombalia WWTP (Figure 1).

As shown in Figure 8, nutrient removal by BW varied depending on the effluent type and the chemical nature of the nutrients. In raw wastewater, NH_4^+ showed the highest removal (32.09%), followed by PO_4^{3-} (16.78%) and NO_3^- (3.30%). This hierarchy reflects the dominant adsorption mechanisms of wood derived biochars. NH_4^+ adsorption occurs mainly through ion exchange and interactions with oxygenated functional groups on the biochar surface [1]. BW, which has a basic pH (9.7), possesses negatively charged surfaces due to carboxylic and phenolic groups, favouring electrostatic attraction of NH_4^+ cations [51]. Nevertheless, the adsorption capacity remained moderate, consistent with literature reporting <20 mg/g for unmodified biochars [1]. The low NO_3^- removal (3.30%) is attributed to electrostatic repulsion between NO_3^- and the negatively charged biochar surface, a well-recognised limitation for unmodified woody biochars [51,52]. Modest phosphate removal (16.78%) likely involves precipitation with metallic cations, particularly calcium and magnesium, present in the wastewater (Table 3) [53,54]. Importantly, the reduction in nutrient uptake compared with synthetic solutions in DI water may be attributed to interference from competing DOC and ions present in much higher concentrations, such as chloride (Table 3). In addition, wastewater cations—including sodium, calcium, and magnesium (Table 3)—and DOC may inhibit NH_4^+- adsorption by competing for available adsorption sites. Furthermore, the wastewater pH (7.5–8) is within the range that enhances NH_4^+- removal but is less favourable for NO_3^- and PO_4^{3-} adsorption, consistent with the trends observed in experiments using synthetic solutions.

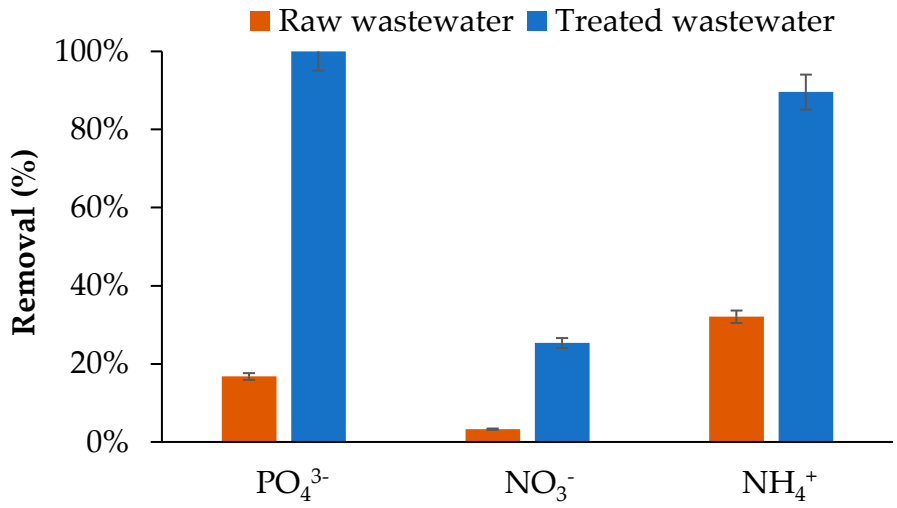

Figure 8. Biochar removal of PO_4^{3-}, NO_3^-, and NH_4^+ in raw and secondary-treated wastewater.

Adsorption performance improved markedly in secondary-treated wastewater, with near-complete phosphate removal (100%) and high NH_4^+ elimination (89.55%), while NO_3^- removal reached 25.38%. This improvement is attributed to higher initial nutrient concentrations, creating favourable concentration gradients for adsorption [55], and to precipitation mechanisms forming calcium or magnesium phosphates on the biochar surface [53–56]. These results demonstrate the strong potential of woodchip biochar for PO_4^{3-} and NH_4^+ removal after secondary treatment, whereas effective NO_3^- removal would require chemical or physical surface modifications to overcome negative surface charge limitations [57].

Compared with other biochar systems treating real wastewater, the observed nutrient removal efficiencies are notable. NH_4^+ removal (89.55%) exceeds the 71% reported for biochar filter columns, and complete PO_4^{3-} removal (100%) surpasses typical values of 57–88% achieved with Mg-Al-modified biochars [58]. In contrast, NO_3^- removal (3.30–25.38%) aligns with previous reports for unmodified biochars (3.6–11.7%), confirming that effective NO_3^- elimination requires advanced surface modification [44].

3.7. Circular Economy Potential and Cost–Benefit Considerations

The biochar-based approach developed in this study aligns strongly with circular economy principles by integrating waste valorisation, nutrient recovery, and material reuse. Low-cost woody waste is first energetically valorised through pyrolysis, producing biochar as a stable carbon-rich adsorbent [59]. Unlike many engineered materials, the produced biochar exhibits an intrinsic capacity to simultaneously adsorb anionic (phosphate and nitrate) and cationic (ammonium) nutrients without chemical or physical pretreatment, thereby reducing process complexity and resource inputs.

After wastewater treatment, the nutrient-loaded biochar can be recycled and reused for soil amendment or for slow-release of fertiliser, enabling recovery of nutrients in plant-available forms [60]. This approach closes the nutrient loop, reduces dependence on synthetic fertilisers, and contributes to carbon sequestration, positioning biochar as both a treatment material and a long-term carbon sink [61].

From a cost–benefit perspective, conventional best-available technologies such as biological nutrient removal, chemical phosphorus precipitation, and membrane-based tertiary treatments are effective but typically associated with high capital expenditure (CAPEX) and high operating expenditure (OPEX) due to infrastructure requirements, energy consumption, chemical inputs, and sludge handling [62]. Moreover, many of these technologies

are destructive, converting nutrients—particularly nitrate through denitrification—into gaseous forms, thereby preventing nutrient recovery and reuse.

Table 8 presents indicative cost ranges reported in the literature for common nutrient-removal technologies and biochar-based adsorption. As shown in Table 8, biological denitrification remains a highly effective and often cost-efficient technology for nitrate removal, particularly in centralised wastewater treatment plants. However, its primary objective is nutrient removal rather than recovery. In contrast, biochar adsorption does not aim to replace biological denitrification but to complement existing treatment trains, especially as a tertiary or polishing step where nutrient recovery, material reuse, and operational simplicity are prioritised.

Table 8. Indicative cost comparison of nutrient removal technologies.

Technology	Indicative Cost Range *	Main Characteristics	References
Biological Nutrient Removal	OPEX: ~259–477 USD per million gallons treated	Effective nitrate removal; high energy demand; nutrient destruction	[62]
Chemical Phosphorus Precipitation	OPEX: ~91–215 USD per million gallons treated	Chemical-intensive; sludge generation; no nutrient recovery	[62]
Membrane Bioreactor	OPEX: ~0.24–0.59 USD per m^3 treated	High energy use; membrane fouling; high CAPEX	[63]
Advanced Membranes	Very high CAPEX and OPEX	Concentrate disposal; energy-intensive	[64]
Biochar adsorption	Biochar production: ~200–400 USD per ton	Low energy input; nutrient recovery; reusable material	[30]

Note: * Indicative values compiled from published technical and techno-economic studies; actual costs depend on plant scale, effluent targets, and local conditions.

The added value of biochar therefore lies not in outperforming conventional technologies on single-nutrient removal efficiency, but in its multi-functional role: simultaneous removal of multiple nutrient species, lower CAPEX and OPEX, reuse of nutrient-loaded material, and fertiliser substitution. These combined benefits make biochar particularly suitable for decentralised, small-scale, or resource-limited wastewater treatment systems.

4. Conclusions

This study shows that woodchip biochar produced at 550 °C is an effective adsorbent for removing PO_4^{3-}, NO_3^-, and NH_4^+ from aqueous solutions. Adsorption was rapid, with approach to equilibrium times were about 20 min for NH_4^+ and 40 min for PO_4^{3-} and NO_3^-. pH strongly influenced performance, favouring NH_4^+-removal under alkaline conditions and anionic PO_4^{3-} and NO_3^- removal under acidic conditions. The pseudo-second-order model best described the adsorption kinetics of the anionic species (NO_3^- and PO_4^{3-}), while the pseudo-first-order model fitted better the data of the cationic species NH_4^+. The Freundlich isotherm fitted the equilibrium data, indicating heterogeneous adsorption. Surface analyses (SEM–EDX, FTIR) confirmed structural and chemical changes consistent with nutrient binding. When applied to real wastewater, biochar performed best in secondary-treated effluent, achieving high removal of NH_4^+ (89.55%) and complete removal of phosphate, though NO_3^- removal remained low.

Importantly, this study highlights the potential of biochar to support circular economy strategies by valorising locally available woody waste to recover nutrients from wastewater in plant-available forms. This has potential to enable the reuse of nutrient-loaded biochar as a soil amendment or slow-release fertiliser, reducing reliance on synthetic fertilisers and contributing to the closure of nutrient loops.

Future work will focus on optimising biochar properties to enhance nitrate (NO_3^-) uptake and evaluating long-term performance under continuous-flow conditions. In addition, forthcoming studies will assess the agricultural application of nutrient-loaded

biochar to demonstrate system effectiveness and to optimise nutrient uptake and release rates, with particular attention to the nitrogen-to-phosphorus (N:P) ratio. Together, these efforts will help bridge the gap between laboratory-scale findings and practical, real-world circular economy applications, supporting both environmental protection and resource sustainability.

Author Contributions: All authors contributed to the study design. A.H.: Investigation, Formal analysis, Writing—original draft. I.T.: Methodology, Formal analysis, Resources, Supervision, Validation, Visualization, Writing—review and editing. C.T.: Methodology, Formal analysis, Visualization, Writing—review and editing. M.A.W.: Methodology, Formal analysis, Visualization, Writing—review and editing. All authors have read and agreed to the published version of the manuscript.

Funding: This work is part of Amani Haddouk's doctoral thesis, funded by the Ministry of Higher Education and Scientific Research, Tunisia.

Data Availability Statement: The original contributions presented in this study are included in the article. Further inquiries can be directed to the corresponding authors.

Conflicts of Interest: The authors declare they have no conflict of interest.

References

1. Zhang, M.; Song, G.; Gelardi, D.L.; Huang, L.; Khan, E.; Mašek, O.; Parikh, S.J.; Ok, Y.S. Evaluating biochar and its modifications for the removal of ammonium, nitrate, and phosphate in water. *Water Res.* **2020**, *186*, 116303. [CrossRef]
2. EPA Harmful Algal Blooms (Habs) in Water Bodies. Available online: https://www.epa.gov/habs (accessed on 1 December 2025).
3. *NT 106.02*; Protection of the Environment—Discharges of Effluents into the Water Environment. Institut National de la Normalisation et de la Propriété Industrielle: Tunis, Tunisia.
4. Yin, Q.; Zhang, B.; Wang, R.; Zhao, Z. Biochar as an adsorbent for inorganic nitrogen and phosphorus removal from water: A review. *Environ. Sci. Pollut. Res.* **2017**, *24*, 26297–26309. [CrossRef]
5. Akinnawo, S.O. Eutrophication: Causes, consequences, physical, chemical and biological techniques for mitigation strategies. *Environ. Chall.* **2023**, *12*, 100733.
6. Chai, H.; Xiang, Y.; Chen, R.; Shao, Z.; Gu, L.; Li, L.; He, Q. Enhanced simultaneous nitrification and denitrification in treating low carbon-to-nitrogen ratio wastewater: Treatment performance and nitrogen removal pathway. *Bioresour. Technol.* **2019**, *280*, 51–58.
7. Burton, F.L.; Tchobanoglus, G.; Metcalf and Eddy, Inc.; Stensel, H.D. *Wastewater Engineering: Treatment and Reuse*; McGraw-HillEducation: Columbus, OH, USA, 2002.
8. Daneshgar, S.; Buttafava, A.; Callegari, A.; Capodaglio, A.G. Economic and energetic assessment of different phosphorus recovery options from aerobic sludge. *J. Clean. Prod.* **2019**, *223*, 729–738. [CrossRef]
9. Gray, H.E.; Powell, T.; Choi, S.; Smith, D.S.; Parker, W.J. Organic phosphorus removal using an integrated advanced oxidation-ultrafiltration process. *Water Res.* **2020**, *182*, 115968. [CrossRef] [PubMed]
10. Deng, Y.; Zhao, R. Advanced oxidation processes (aops) in wastewater treatment. *Curr. Pollut. Rep.* **2015**, *1*, 167–176. [CrossRef]
11. Xie, M.; Shon, H.K.; Gray, S.R.; Elimelech, M. Membrane-based processes for wastewater nutrient recovery: Technology, challenges, and future direction. *Water Res.* **2016**, *89*, 210–221. [CrossRef]
12. Wahab, M.A.; Boubakri, H.; Jellali, S.; Jedidi, N. Characterization of ammonium retention processes onto cactus leaves fibers using ftir, edx and sem analysis. *J. Hazard. Mater.* **2012**, *241–242*, 101–109. [CrossRef]
13. Satyam, S.; Patra, S. Innovations and challenges in adsorption-based wastewater remediation: A comprehensive review. *Heliyon* **2024**, *10*, e29573. [CrossRef]
14. Trivedi, Y.; Sharma, M.; Mishra, R.K.; Sharma, A.; Joshi, J.; Gupta, A.B.; Achintya, B.; Shah, K.; Vuppaladadiyamd, A.K. Biochar potential for pollutant removal during wastewater treatment: A comprehensive review of separation mechanisms, technological integration, and process analysis. *Desalination* **2025**, *600*, 118509. [CrossRef]
15. Wahab, M.A.; Kebelmann, K.; Schartel, B.; Griffiths, G. Improving bio-oil chemical profile of seaweeds through anaerobic fermentation pre-treatment. *Energy Convers. Manag.* **2021**, *245*, 114632. [CrossRef]
16. Cantrell, K.B.; Hunt, P.G.; Uchimiya, M.; Novak, J.M.; Ro, K.S. Impact of pyrolysis temperature and manure source on physicochemical characteristics of biochar. *Bioresour. Technol.* **2012**, *107*, 419–428. [CrossRef]
17. Chen, X.; Chen, G.; Chen, L.; Chen, Y.; Lehmann, J.; McBride, M.B.; Hay, A.G. Adsorption of copper and zinc by biochars produced from pyrolysis of hardwood and corn straw in aqueous solution. *Bioresour. Technol.* **2011**, *102*, 8877–8884. [CrossRef] [PubMed]

18. *ASTM D7582-15*; Standard Test Methods for Proximate Analysis of Coal and Coke by Macro Thermogravimetric Analysis. ASTM-International: Conshohocken, PA, USA, 2015.
19. Cui, X.; Wang, J.; Wang, X.; Khan, M.B.; Lu, M.; Khan, K.Y.; Song, Y.; He, Z.; Yang, X.; Yan, B.; et al. Biochar from constructed wetland biomass waste: A review of its potential and challenges. *Chemosphere* **2022**, *287*, 132259. [CrossRef]
20. Du, Q.; Liu, S.; Cao, Z.; Wang, Y. Ammonia removal from aqueous solution using natural chinese clinoptilolite. *Sep. Purif. Technol.* **2005**, *44*, 229–234. [CrossRef]
21. Hou, J.; Huang, L.; Yang, Z.; Zhao, Y.; Deng, C.; Chen, Y.; Li, X. Adsorption of ammonium on biochar prepared from giant reed. *Environ. Sci. Pollut. Res.* **2016**, *23*, 19107–19115. [CrossRef] [PubMed]
22. Cui, X.; Hao, H.; Zhang, C.; He, Z.; Yang, X. Capacity and mechanisms of ammonium and cadmium sorption on different wetland-plant derived biochars. *Sci. Total Environ.* **2016**, *539*, 566–575. [PubMed]
23. Xue, L.; Gao, B.; Wan, Y.; Fang, J.; Wang, S.; Li, Y.; Muñoz-Carpena, R.; Yang, L. High efficiency and selectivity of mgfe-ldh modified wheat-straw biochar in the removal of nitrate from aqueous solutions. *J. Taiwan Inst. Chem. Eng.* **2016**, *63*, 312–317. [CrossRef]
24. Wang, Z.; Guo, H.; Shen, F.; Yang, G.; Zhang, Y.; Zeng, Y.; Wang, L.; Xiao, H.; Deng, S. Biochar produced from oak sawdust by lanthanum (La)-involved pyrolysis for adsorption of ammonium (NH_4^+), nitrate (NO_3^-), and phosphate (PO_4^{3-}). *Chemosphere* **2015**, *119*, 646–653. [CrossRef]
25. Michálеková-Richveisová, B.; Frišták, V.; Pipíška, M.; Ďuriška, L.; Moreno-Jimenez, E.; Soja, G. Iron-impregnated biochars as effective phosphate sorption materials. *Environ. Sci. Pollut. Res. Int.* **2017**, *24*, 463–475. [CrossRef]
26. Jung, K.W.; Hwang, M.J.; Ahn, K.H.; Ok, Y.S. Kinetic study on phosphate removal from aqueous solution by biochar derived from peanut shell as renewable adsorptive media. *Int. J. Environ. Sci. Technol.* **2015**, *12*, 3363–3372. [CrossRef]
27. Wahab, M.A.; Jellali, S.; Jedidi, N. Effect of temperature and ph on the biosorption of ammonium onto posidonia oceanica fibers: Equilibrium, and kinetic modeling studies. *Bioresour. Technol.* **2010**, *101*, 8606–8615. [CrossRef]
28. Chintala, R.; Mollinedo, J.; Schumacher, T.E.; Papiernik, S.K.; Malo, D.D.; Clay, D.E.; Kumar, S.; Gulbrandson, D.W. Nitrate sorption and desorption in biochars from fast pyrolysis. *Microporous Mesoporous Mater.* **2013**, *179*, 250–257. [CrossRef]
29. Wahab, M.A.; Jellali, S.; Jedidi, N. Ammonium biosorption onto sawdust: Ftir analysis, kinetics and adsorption isotherms modeling. *Bioresour. Technol.* **2010**, *101*, 5070–5075. [CrossRef]
30. Tan, X.; Liu, Y.; Zeng, G.; Wang, X.; Hu, X.; Gu, Y.; Yang, Z. Application of biochar for the removal of pollutants from aqueous solutions. *Chemosphere* **2015**, *125*, 70–85. [CrossRef] [PubMed]
31. Yunis, R.; Imran, M.; Mitu, L.; Kanwal, F. Adsorption studies of flourescein on roots, stem and leaves of phoenix dactylifera. *Asian J. Chem.* **2010**, *23*, 345–350.
32. Vu, T.M.; Phuong Nguyen, T.M.; Van, H.-T.; Le, N.T.; Tran, D.-T. Biomass-derived hydrochar and activated carbon in pharmaceutical pollution mitigation: A comprehensive overview. *RSC Adv.* **2025**, *15*, 43053–43084. [CrossRef] [PubMed]
33. Plazinski, W.; Dziuba, J.; Rudzinski, W. Modeling of sorption kinetics: The pseudo-second order equation and the sorbate intraparticle diffusivity. *Adsorption* **2013**, *19*, 1055–1064. [CrossRef]
34. Wu, X.; Ye, M.; Wang, J.; Wu, F.; Liu, C.; Li, Z.; Lin, D.; Yang, R. Adsorption characteristics and mechanism of ammonia nitrogen and phosphate from biogas slurry by Ca^{2+}-modified soybean straw biochar. *PLoS ONE* **2023**, *18*, e0290714. [CrossRef]
35. Gong, Y.-P.; Ni, Z.-Y.; Xiong, Z.-Z.; Cheng, L.-H.; Xu, X.-H. Phosphate and ammonium adsorption of the modified biochar based on phragmites australis after phytoremediation. *Environ. Sci. Pollut. Res.* **2017**, *24*, 8326–8335. [CrossRef]
36. Hu, X.; Zhang, X.; Ngo, H.H.; Guo, W.; Wen, H.; Li, C.; Zhang, Y.; Ma, C. Comparison study on the ammonium adsorption of the biochars derived from different kinds of fruit peel. *Sci. Total Environ.* **2020**, *707*, 135544.
37. Biswas, B.; Adhikari, S.; Jahromi, H.; Ammar, M.; Baltrusaitis, J.; Torbert, A.; Linhoss, J.; Lamba, J. Magnesium doped biochar for simultaneous adsorption of phosphate and nitrogen ions from aqueous solution. *Chemosphere* **2024**, *358*, 142130. [CrossRef]
38. Xia, S.; Liang, S.; Qin, Y.; Chen, W.; Xue, B.; Zhang, B.; Xu, G. Significant improvement of adsorption for phosphate removal by lanthanum-loaded biochar. *ACS Omega* **2023**, *8*, 24853–24864. [CrossRef] [PubMed]
39. Manawi, Y.; Al-Gaashani, R.; Simson, S.; Tong, Y.; Lawler, J.; Kochkodan, V. Adsorptive removal of phosphate from water with biochar from acacia tree modified with iron and magnesium oxides. *Sci. Rep.* **2024**, *14*, 17414. [CrossRef]
40. Li, Z.; Huang, J.; Zhang, W.; Yu, H.; Wang, Y. Simultaneous decontamination for ammonia nitrogen and phosphate efficiently by crystal morphology mgo-coated functional biochar derived from sludge and sunflower stalk. *Toxics* **2025**, *13*, 577. [CrossRef]
41. Haghighi Mood, S.; Ayiania, M.; Cao, H.; Marin-Flores, O.; Milan, Y.J.; Garcia-Perez, M. Nitrogen and magnesium co-doped biochar for phosphate adsorption. *Biomass Convers. Biorefinery* **2024**, *14*, 5923–5942.
42. Fidel, R.B.; Laird, D.A.; Spokas, K.A. Sorption of ammonium and nitrate to biochars is electrostatic and ph-dependent. *Sci. Rep.* **2018**, *8*, 17627. [CrossRef] [PubMed]
43. Zhang, M.; Gao, B.; Yao, Y.; Xue, Y.; Inyang, M. Synthesis of porous mgo-biochar nanocomposites for removal of phosphate and nitrate from aqueous solutions. *Chem. Eng. J.* **2012**, *210*, 26–32.

44. Ilić, M.; Haegel, F.H.; Lolić, A.; Nedić, Z.; Tosti, T.; Ignjatović, I.S.; Linden, A.; Jablonowski, N.D.; Hartmann, H. Surface functional groups and degree of carbonization of selected chars from different processes and feedstock. *PLoS ONE* **2022**, *17*, e0277365. [CrossRef]
45. Saini, P.; de Koff, J.P.; Rakshit, S. In situ atr-ftir spectroscopy for evidencing the adsorption mechanism of ammonium on a pinewood-derived biochar. *Agric. Environ. Lett.* **2023**, *8*, e20097. [CrossRef]
46. Fan, R.; Chen, C.L.; Lin, J.Y.; Tzeng, J.H.; Huang, C.P.; Dong, C.; Huang, C.P. Adsorption characteristics of ammonium ion onto hydrous biochars in dilute aqueous solutions. *Bioresour. Technol.* **2019**, *272*, 465–472. [CrossRef] [PubMed]
47. Shenk, A.; Ivan, J.-P.A.; Schwede, S.; Odlare, M. Analysis of influencing characteristics of biochars for ammonium adsorption. *Appl. Sci.* **2022**, *12*, 9487. [CrossRef]
48. Deng, Y.; Li, M.; Zhang, Z.; Liu, Q.; Jiang, K.; Tian, J.; Zhang, Y.; Ni, F. Comparative study on characteristics and mechanism of phosphate adsorption on mg/al modified biochar. *J. Environ. Chem. Eng.* **2021**, *9*, 105079. [CrossRef]
49. Muscarella, S.M.; Di Trapani, D.; Laudicina, V.A.; Mannina, G. Phosphorus recovery from ultrafiltered membrane wastewater by biochar adsorption columns: The effect of loading rates. *Heliyon* **2024**, *10*, e34659. [CrossRef]
50. Xing, W.; Zong, T.; Sun, Y.; Fang, W.; Shen, T.; Zhou, Y. Nano-biochar enhanced adsorption of NO_3^--N and its role in mitigating N_2O emissions: Performance and mechanisms. *Agronomy* **2025**, *15*, 1723. [CrossRef]
51. Hollister, C.C.; Bisogni, J.J.; Lehmann, J. Ammonium, nitrate, and phosphate sorption to and solute leaching from biochars prepared from corn stover (*Zea mays* L.) and oak wood (*Quercus* spp.). *J. Environ. Qual.* **2013**, *42*, 137–144. [CrossRef]
52. Gai, X.; Wang, H.; Liu, J.; Zhai, L.; Liu, S.; Ren, T.; Liu, H. Effects of feedstock and pyrolysis temperature on biochar adsorption of ammonium and nitrate. *PLoS ONE* **2014**, *9*, e113888. [CrossRef]
53. Yao, Y.; Gao, B.; Chen, J.; Yang, L. Engineered biochar reclaiming phosphate from aqueous solutions: Mechanisms and potential application as a slow-release fertilizer. *Environ. Sci. Technol.* **2013**, *47*, 8700–8708. [CrossRef] [PubMed]
54. Fang, C.; Zhang, T.; Li, P.; Jiang, R.-F.; Wang, Y.-C. Application of magnesium modified corn biochar for phosphorus removal and recovery from swine wastewater. *Int. J. Environ. Res. Public Health* **2014**, *11*, 9217–9237. [CrossRef]
55. Pantoja, F.; Sukmana, H.; Beszédes, S.; László, Z. Removal of ammonium and phosphates from aqueous solutions by biochar produced from agricultural waste. *J. Mater. Cycles Waste Manag.* **2023**, *25*, 1921–1934. [CrossRef]
56. Li, A.; Ge, W.; Liu, L.; Qiu, G. Preparation, adsorption performance and mechanism of mgo-loaded biochar in wastewater treatment: A review. *Environ. Res.* **2022**, *212*, 113341. [CrossRef] [PubMed]
57. Shakoor, M.B.; Ye, Z.-L.; Chen, S. Engineered biochars for recovering phosphate and ammonium from wastewater: A review. *Sci. Total Environ.* **2021**, *779*, 146240. [CrossRef]
58. Yin, Q.; Ren, H.; Wang, R.; Zhao, Z. Evaluation of nitrate and phosphate adsorption on al-modified biochar: Influence of al content. *Sci. Total Environ.* **2018**, *631–632*, 895–903. [CrossRef]
59. Lehmann, J.; Joseph, S. *Biochar for Environmental Management: Science, Technology and Implementation*, 2nd ed.; Routledge: London, UK, 2015. [CrossRef]
60. Agegnehu, G.; Bass, A.M.; Nelson, P.N.; Bird, M.I. Benefits of biochar, compost and biochar-compost for soil quality, maize yield and greenhouse gas emissions in a tropical agricultural soil. *Sci. Total Environ.* **2016**, *543*, 295–306. [PubMed]
61. Woolf, D.; Amonette, J.E.; Street-Perrott, F.A.; Lehmann, J.; Joseph, S. Sustainable biochar to mitigate global climate change. *Nat. Commun.* **2010**, *1*, 56. [CrossRef]
62. EPA Municipal Nutrient Removal Technologies Reference Document. Available online: https://www.epa.gov/sustainable-water-infrastructure/municipal-nutrient-removal-technologies-reference-document (accessed on 1 September 2024).
63. Krzeminski, P.; van der Graaf, J.H.; van Lier, J.B. Specific energy consumption of membrane bioreactor (mbr) for sewage treatment. *Water Sci. Technol.* **2012**, *65*, 380–392. [CrossRef]
64. Shannon, M.A.; Bohn, P.W.; Elimelech, M.; Georgiadis, J.G.; Mariñas, B.J.; Mayes, A.M. Science and technology for water purification in the coming decades. *Nature* **2008**, *452*, 301–310. [CrossRef]